Journal of Geosciences, 58 (2013), 379–396 DOI: 10.3190/jgeosci.154

Original paper

Geology, mineralogy and the Pb, S isotope study of the Kalkım Pb–Zn ± Cu deposits, Biga Peninsula, NW Turkey

Sinan AKISKA[1]*, Gökhan DEMIRELA[2], Sönmez I. SAYILI[3]

[1] *Ankara Üniversitesi, Mühendislik Fakültesi, Jeoloji Mühendisliği Bölümü, TR-06100, Tandoğan, Ankara, Turkey; akiska@eng.ankara.edu.tr*
[2] *Aksaray Üniversitesi, Mühendislik Fakültesi, Jeoloji Mühendisliği Bölümü, TR-68100, Aksaray, Turkey*
[3] *Fe–Ni Madencilik, Ceyhun Atıf Kansu Caddesi, 1368 Sokak, No: 6/4 Balgat, Ankara, Turkey*
* *Corresponding author*

Three main Pb–Zn ± Cu deposits (Handeresi, Bağırkaçdere, and Fırıncıkdere) occur south of Kalkım in the southeastern part of the Biga Peninsula (NW Turkey). Massive and disseminated Pb–Zn mineralization consists of ore veins in fault zones and replacement bodies in carbonate layers in metamorphic rocks. Garnet (~$Ad_{64}Gr_{36}$), pyroxene (~$Di_{30}Hd_{45}Jo_{25}$), epidote and rare tremolite–actinolite are found as gangue minerals in ore zones. The garnets often show oscillatory zoning and correspond to grossular, andradite and grandite in composition. The pyroxene minerals are manganiferous hedenbergite, johannsenite and diopside. The Mn/Fe ratios of the pyroxene range between 0.3 and 0.9 (mean 0.5). Such compositions of the garnet and pyroxene and gangue assemblages are typical of distal Pb–Zn skarns. The ore minerals are pyrite, sphalerite, chalcopyrite, galena, magnetite, hematite, and arsenopyrite.

The mean lead isotopic values for galena are $^{206}Pb/^{204}Pb \sim 18.760$, $^{207}Pb/^{204}Pb \sim 15.689$, and $^{208}Pb/^{204}Pb \sim 38.935$. The comparison of these isotope data with the host-rock samples (graphite schist, andesite and granodiorite) indicates that part of lead could have been leached from the schists. The $\delta^{34}S_{VCDT}$ values for galena, sphalerite, and chalcopyrite are –1.1 to +1.5 ‰ (mean: –0.2 ‰), 0.7 to +2. 1 ‰ (mean: +0.7 ‰), and –0.6 to +1.5 ‰ (mean: +0.4 ‰), respectively. Lead isotope data and $\delta^{34}S_{VCDT}$ values close to 0 ‰ indicate the formation of ores by magmatic processes.

Taken together, the Oligo–Miocene magmatism in the area is taken responsible for the polymetallic mineralization. However, the metamorphic rocks and their protoliths may have contributed part of the lead.

Keywords: lead–zinc mineralization, skarn, sulphur and lead isotopes, Handeresi, Bağırkaçdere, Fırıncıkdere
Received: 11 June 2013; accepted: 2 November 2013; handling editor: M. Štemprok

1. Introduction

In the Biga Peninsula (NW Turkey), many Pb–Zn deposits are located besides the uneconomic Cu–Mo–W–Au and Ag occurrences. The Handeresi, Bağırkaçdere and Fırıncıkdere (HBF) deposits are the most important sources of Pb–Zn ± Cu in Turkey with total mineral resources of 8.7 mt at an average grade of 7 % Pb, 4 % Zn and 3000 g/t Cu (Yücelay 1976; Çetinkaya et al. 1983a, b). The HBF deposits were discovered in the early 1970s by the General Directorate of Mineral Research and Exploration of Turkey (MTA) using stream geochemistry, geophysical methods, and drilling. A number of domestic and foreign mining companies actively operate in the area. However, the discovery of Pb, Zn, Ag and Au in ancient galleries from the Trojan and Ottoman periods shows that the Biga Peninsula was an important mining centre in ancient times as well.

The lead–zinc deposits of the Biga Peninsula are characterized by two principal genetic types: (1) skarn-carbonate replacement deposits (CRD) bound to carbonate lenses in metamorphic rocks (biotite, chlorite, sericite–graphite schist, phyllite and metasandstone), and (2) vein type Pb–Zn mineralization related to fractures in volcanic and metamorphic rocks (Demirela 2011).

The ore deposits of Biga Peninsula were investigated by Yücelay (1976) and Çetinkaya et al. (1983a, b); however, these authors focused mainly on ore geology and mineralogy. The genesis of the deposits and the source of metals remain unconstrained by modern analytical methods. In our study by electron microprobe and Pb–S isotope techniques, we concentrate on ore geology as well as the likely source of fluids and metals for ore-forming processes.

2. Regional geological setting

The geological and geodynamic history of Biga Peninsula and its surroundings have been studied by Krushensky et al. (1971), Bingöl (1976), Okay et al. (1990), Okay and Tüysüz (1999), Delaloye and Bingöl (2000), and Cavazza et al. (2009). According to Ketin (1966), the area enclosing the HBF deposits is located in the

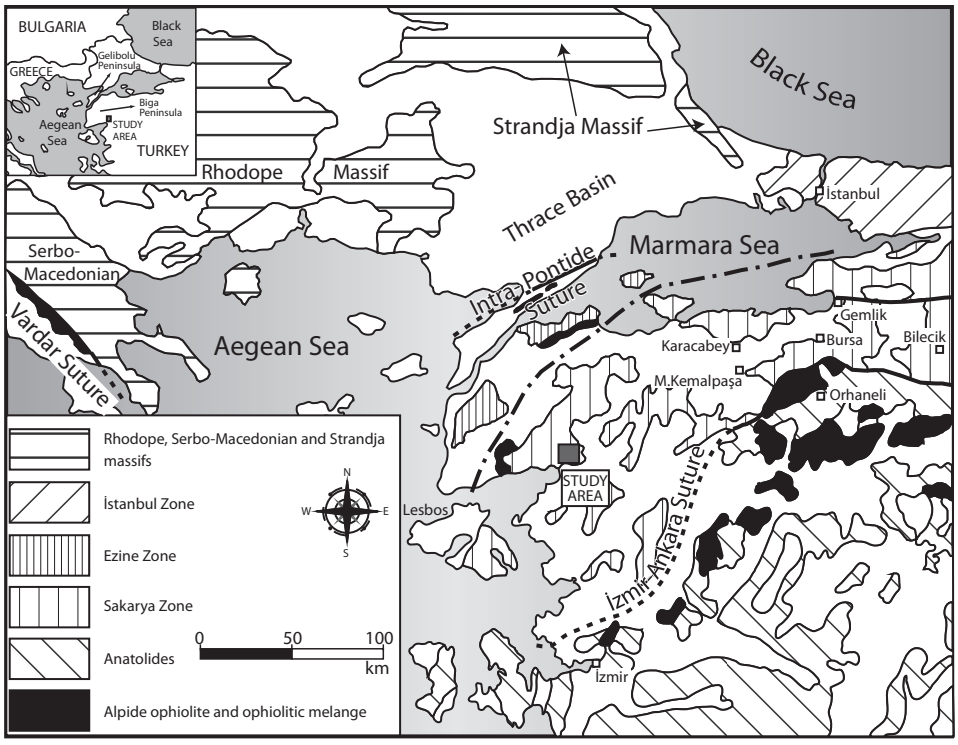

Fig. 1 Geotectonic map of the Biga Peninsula and its surroundings. White areas indicate the post-tectonic Tertiary rocks, the dash-dot line shows the probable location of the Palaeo-Tethys suture (Okay et al. 1990).

northwestern part of the Pontide geotectonic unit. Four pre-Tertiary tectonic zones were distinguished in the Gelibolu–Biga peninsulas (Okay et al. 1990): Gelibolu, Ezine, Ayvacık, and Sakarya zones (from northeast to southwest; Fig. 1). The Sakarya Continent (as defined by Şengör and Yılmaz 1981) is limited by the Intra-Pontide Suture in the north and by the İzmir–Ankara Suture in the south. A highly deformed and metamorphosed pre-Jurassic basement and much less deformed and/or unmetamorphosed Jurassic–Tertiary cover have been distinguished (Okay et al. 2008). Pre-Jurassic metamorphosed basement in the study area is represented by the Çamlık granodiorite and by the Kalabak Fm.

The Çamlık granodiorite crops out in two areas (Fig. 2). Yücelay (1976), Çetinkaya et al. (1983a, b), and Tufan (1993) examined the study area with regard to mining geology and Okay et al. (1990, 1996, 2006) and Aysal et al. (2012) studied the geological and the tectonic evolution. Tufan (1993) and Okay et al. (1996) observed a tectonic contact between granodiorite and epidote–sericite–graphite schist, metasandstone, and the marble which was metamorphosed together with country rocks. According to Tufan (1993), there is no contact metamorphism between the granodiorite and Kalabak Fm. It is thus likely that the Çamlık granodiorite intruded before sedimentation of the Kalabak Fm. and that the both units were metamorphosed jointly. The granodiorite is 399 ± 13 Ma old (Pb–Pb single-zircon evaporation technique; Okay et al. 1996). The Neogene extensional regime and right-lateral strike-slip faulting, which occurred in the region after Miocene, obscured the relationships among the pre-Eocene units (Okay et al. 1996). In contrast to this view, Aysal et al. (2012) reported that the Çamlık granodiorite intruded into the Kalabak Fm. and these units were named as the Havran Unit.

Precambrian units of the Kazdağ Massif are overlain by the Kalabak Fm. outside the study area. The Çamlık granodiorite occurs in the north and by an angular unconformity the Kalkım volcanics and Akköy Fm. (Tufan 1993) overlays the Kalabak Fm. The Kalabak Fm. was studied in detail by Yücelay (1976), Çetinkaya et al. (1983a, b) and Tufan (1993). The Kalabak Fm. consists of biotite, sericite–chlorite, chlorite, and sericite–graphite schists, metasandstone, marble or serpentinite lenses and metadiabase bodies.

The Biga Peninsula was uplifted at the end of Oligocene, when the terrestrial regime predominated and the Eocene–Oligocene successions were substantially eroded (Okay et al. 1990). After this stage, an intense calc-alkaline magmatism occurred during Late Oligocene to Early Miocene times. In the southern part of the Biga Peninsula, the following cooling ages were determined for the Eybek Pluton (23.5 ± 0.6, K–Ar biotite, 24.2 ± 0.9 Ma, K–Ar hornblende, Krushensky 1975), 23.9 ± 1.2 – 30.5 ± 2.2 Ma (K–Ar biotite and whole rock, Ayan 1979), Kestanbol syenite (28 ± 0.88 Ma, K–Ar whole rock, Fytikas et al. 1976; 20.5 ± 0.6 Ma, K–Ar hornblende, Delaloye and Bingöl 2000) and Nevruz-Çakıroba granodiorite (24.1 ± 0.5 Ma, K–Ar hornblende and whole rock, Zimmermann et al. 1989).

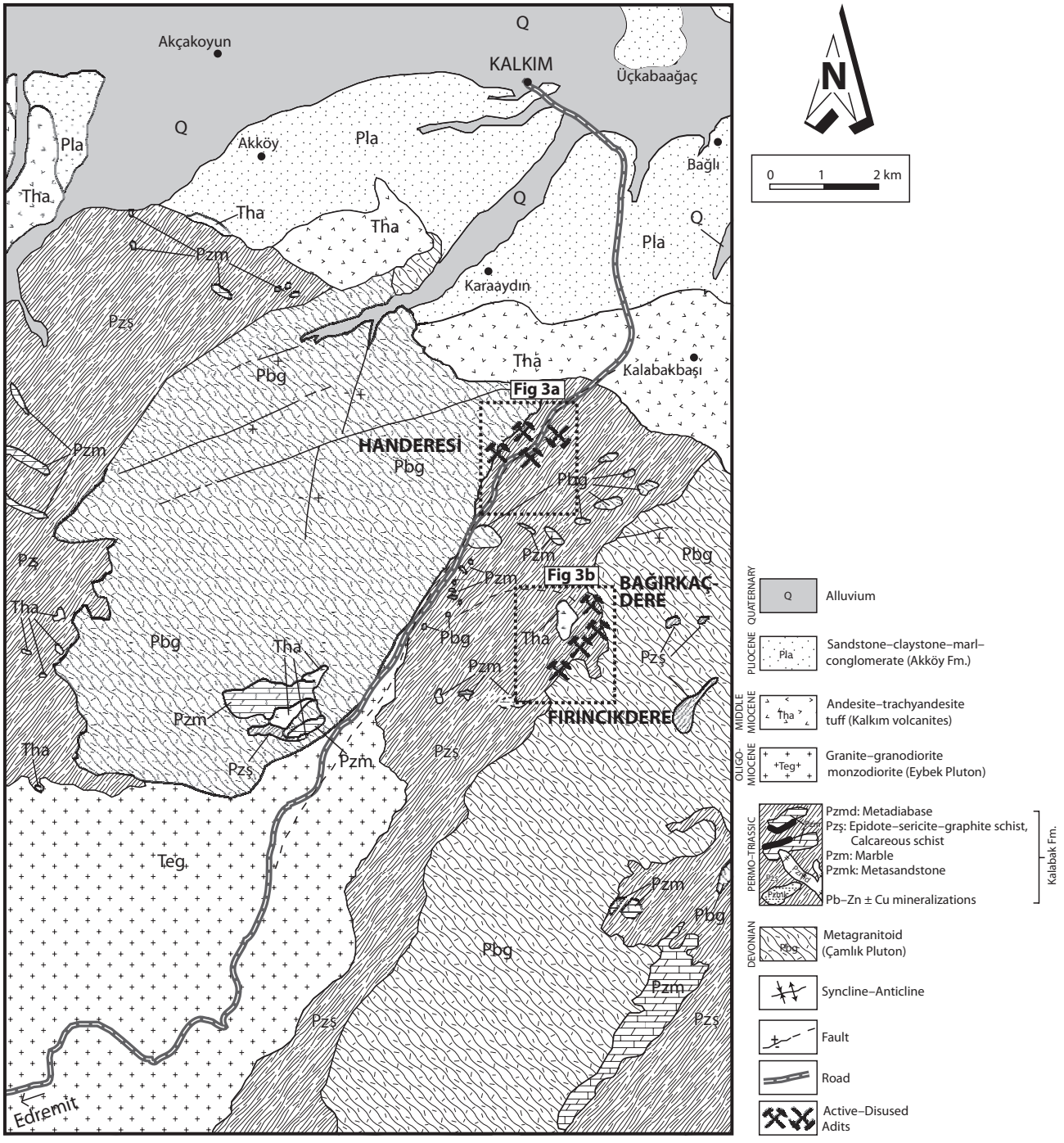

Fig. 2 Geological map of the study areas (modified from Duru et al. 2007).

The Eybek Pluton (*c*. 90 km^2) intruded the outer metamorphic units of the Kazdağ Massif (Fig. 2). In the study area, it is formed by granite, granodiorite and monzodiorite. Dikes of younger granophyres (trending N–S, NW–SE and NE–SW) occur especially in the eastern part of the Pluton. During Early–Middle Miocene, a massive volcanism produced andesites, dacite breccias, trachytes, trachyandesites and basalts (Ercan 1979; Tufan 1993). Kalkım volcanics (Hallaçlar Fm.: Krushensky 1975) are overlain by the Akköy Fm. with angular discordance in the north, unconformably covering the Çamlık granodiorite and the Kalabak Fm. (Tufan 1993) (Fig. 2). They are represented by ignimbrites, tuffs and agglomerates of rhyolite, dacite, andesite and trachyandesite composition.

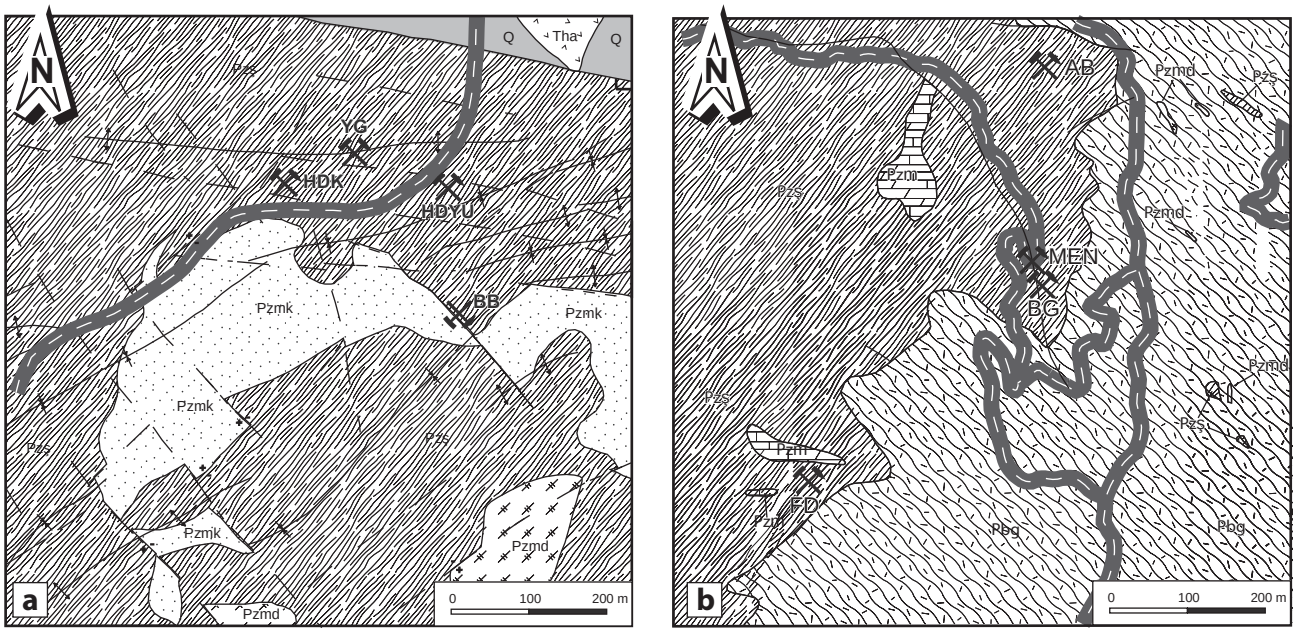

Fig. 3a – The geological map of Handeresi area (modified from Yücelay 1976). **b** – The geological map of Bağırkaçdere and Fırıncıkdere areas (modified from Çetinkaya et. al. 1983a), (see Fig. 2 for the legend).

3. Mineral deposits

The ore bodies in the HBF deposits are hosted by carbonate layers in Permo–Triassic calcareous schists or occur in veins cutting these rocks. The approximate sizes of the orebodies range from a few cm to 40–50 cm in width and *c.* 500 m in length in all areas. In the study area, Kalkım volcanics and Eybek intrusion are located northeast and

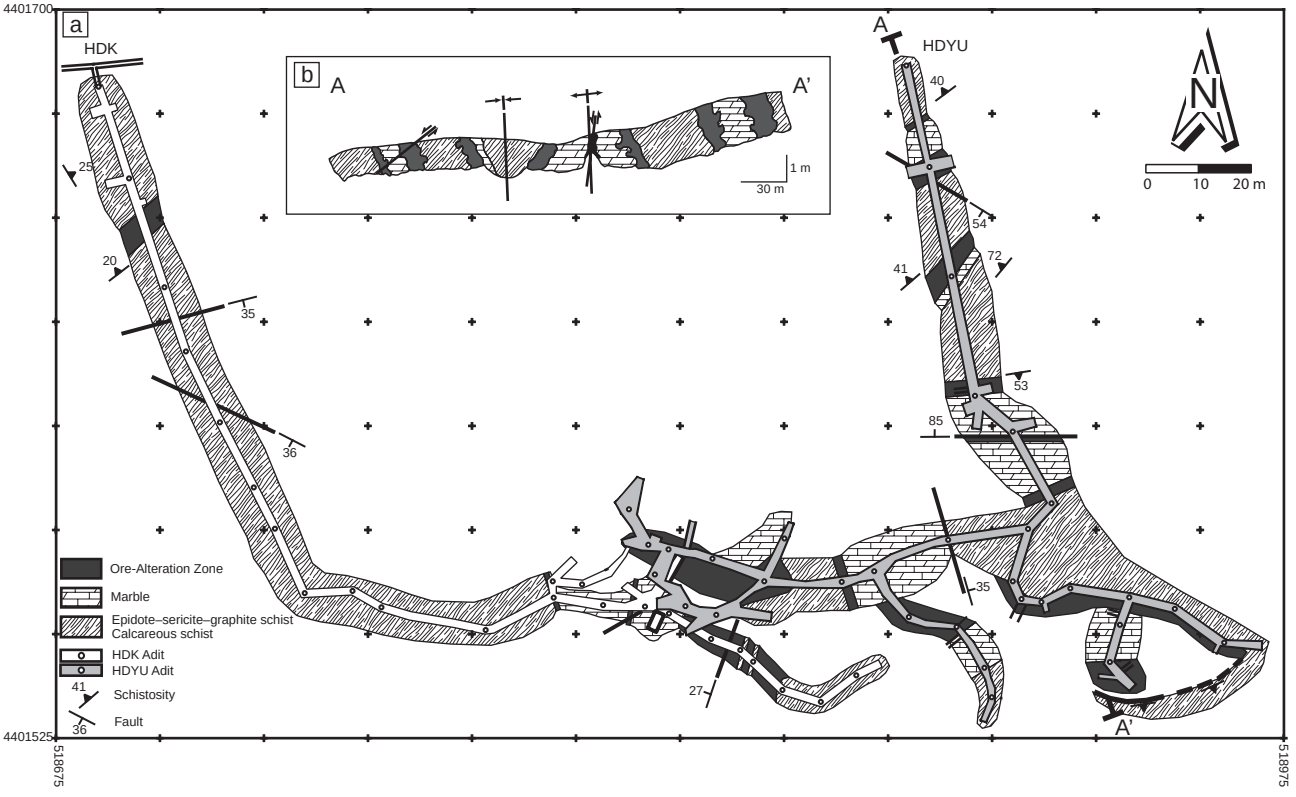

Fig. 4a – Geological map of Handeresi Dere Kenarı (HDK) adit (Level: 280 m) and Handeresi Yol Üstü (HDYU) adit (Level: 295 m) in Handeresi area (Akıska 2010). **b** – Geological cross-section along lines A–A' (coordinates are given in UTM coordinate system – Zone 35S).

southwest of these deposits, respectively. Based on the field relations and studies of boreholes (up to 245 m deep), there is no apparent spatial association between the ore zones and igneous rocks.

3.1. Handeresi area

Handeresi area is located 10 km S of Kalkım. Four adits explored the area with a total length of *c.* 900 m. Epidote–sericite–graphite schist, metasandstone, metadiabase, quartzite, and marble are the most common host rocks. The ore occurs along the contacts between the marble and the schists (calcareous and graphite-bearing) and in fractures (Fig. 3a). Major faults as well as individual ore zones strike usually NE–SW. The faulting was probably associated with regional folding. The schistosity created suitable planes for location of the ore bodies. While the schistosity strikes generally to the NE, the dip ranges between 20 and 72° NW. The strike is rarely N30°W with a dip 25°NE (Fig. 4a–b).

3.2. Bagırkaçdere area

The Bağırkaçdere area is situated 15 km south–southeast of Kalkım. Three adits (total length of ~1100 m) were excavated here. The metamorphic sequence is represented by schists (calcareous and graphite-bearing), metasandstone and marble lenses (hosting the ore bodies; Fig. 3b). The general trend of faults and of many ore zones is NW–SE. The strike and dip of schistosity are *c.* N60°W, 45°NE (Fig. 5a–b). The main mineralized zone in the Bağırkaçdere adit (BG) strikes NW–SE. Schistosity planes and the parallel faults controlled the ore deposition.

3.3. Fırıncıkdere area

The Fırıncıkdere area is situated 15–20 km south of Kalkım. One adit 365 m long was made in the area and has been used for mining. The main geological and structural setting is the same as at the above two localities.

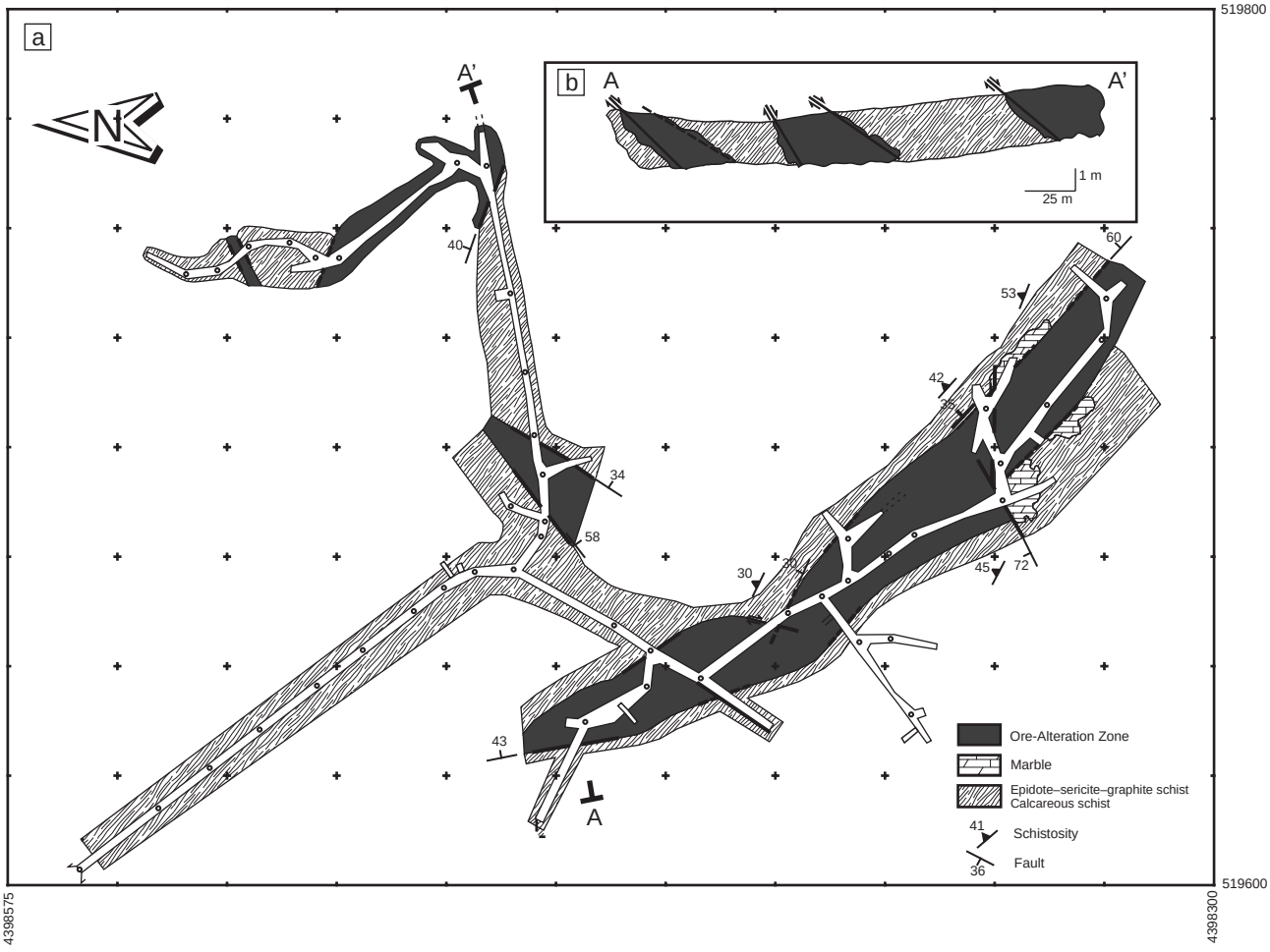

Fig. 5a – Geological map of Bağırkaçdere (BG) adit (Level: 570 m) in Bağırkaçdere area (Akıska 2010). **b** – Geological cross-section along lines A–A' (coordinates are given in UTM coordinate system – Zone 35S).

While the strikes of faults are NW–SE and NE–SW, the strike of schistosity ranges 10–75º NE and the dip 28–40º SE (Fig. 3b). The textural and structural features and the relations of wall-rocks to mineralization are identical in the three areas.

4. Analytical methods

4.1. Mineral chemistry

The mineralogical and petrographical studies were carried out on 220 samples, 238 thin sections and 23 polished sections. Mineral composition of sulphide minerals was determined using JEOL JXA-8900R electron probe microanalyzer (EPMA) in Electron Microanalysis & Imaging Laboratory (EMIL) at the University of Nevada in Las Vegas (UNLV). Analyses were conducted with a 20 kV accelerating voltage, 10 nA current, and 5 µm beam diameter. Natural mineral standards were utilized for the following elements: As (FeAsS), Fe and S (FeS_2), Zn (ZnS), Hg (HgS) and Cu ($CuFeS_2$). Pure metals were used as standards for Co and Ni. Counting times were 30 s on peak and background for all elements except Co and Ni, for which counting times were 40 s on peak and background.

Semi-quantitative analyses of fine-grained fibrous sulphides were conducted using JEOL JSA-5600 scanning electron microscope equipped with an Oxford Link Pentafet 6587 energy dispersive X-ray spectrometer at UNLV. The analyses were conducted at 15kV, with a 20 mm working distance, a spot size of 40 µm, and acquisition times of 60 s. Analyses are reported as normalized weight percentages.

Mineral composition of silicate minerals was studied using JEOL JXA-8900R electron probe microanalyzer at UNLV. Garnet analyses were conducted at 15 kV accelerating voltage, 10 nA current, and 1 µm beam diameter. Natural mineral standards used were: Si and Al (pyrope), Ti (ilmenite), Cr (chromite), Fe (almandine), Mg (forsterite), Mn (rhodonite), and Ca (wollastonite). Pyroxene analyses were conducted at 15 kV accelerating voltage, 10 nA current, and 5 µm beam diameter using the following standards: Si and Na (albite), Al (sillimanite), Fe and Ti (ilmenite), Mg (enstatite), Mn (rhodonite), Ca (wollastonite) and K (orthoclase). Counting times were 30 s on peak and background for all elements.

4.2. Sulphur isotopes

Samples selected for isotope analyses (both S and Pb) were first grinded and sieved to a mesh size of 2 mm. Individual minerals were then separated in heavy liquids. Finally, individual grains were handpicked under the binocular microscope. The $\delta^{34}S$ values were measured in SO_2 gas using a continuous-flow gas-ratio mass spectrometer (ThermoQuest Finnigan Delta PlusXL) in Environmental Isotope Laboratory at the University of Arizona. Samples for sulphur isotopic determinations were then combusted at 1030 °C in oxygen (O_2 or V_2O_5) and carried out using an elemental analyser (Costech) coupled to the mass spectrometer. Standardization was based on international standards OGS-1 and NBS123, and several other sulphide and sulphate materials that have been compared between laboratories. The data are presented in delta (δ) notation as per mill (‰) deviations relative to the Vienna Canyon Diablo Triolite (VCDT) standard for sulphur. Calibration is linear in the range –10 to +30 ‰. Precision is estimated to be ± 0.15 ‰ or better (1σ), based on repeated measurement of internal standards.

4.3. Lead isotopes

Lead isotope analyses of both galena and host-rock samples were carried out by the Australian Laboratory Service (ALS Scandinavia AB) in Sweden. Sample preparation consisted in MW-assisted digestion in Teflon vessels using a HNO_3/HF mixture followed by dilution of digests in 0.7M HNO_3 to final Pb concentration of 50 ± 5 µg/L. Two aliquots were prepared for each sample. The Pb isotope ratio measurements were performed by Inductively Coupled Plasma-Sector Field Mass Spectrometry (MC-ICP-SFMS) using combination of internal standardization (Tl added to all solutions) and bracketing standards (NIST NBS 981) in order to correct for instrumental mass-bias. Isotopes ^{201}Hg, ^{203}Tl, $^{204}Pb + {}^{204}Hg$, ^{205}Tl, ^{206}Pb, ^{207}Pb and ^{208}Pb were monitored using 10% acquisition, search and integration windows (thus taking advantage of 'flat-top' peak shape offered by ICP-SFMS), 1 ms setting and 2 ms sample times, analogue detector mode and 4500 scans (3 runs of 1500 replicates) in each measured solution. Measurement accuracy was assessed by NIST NBS 981 diluted to 50 µg/L and analysed as test sample at the beginning and in the end of analytical sequence and was found to be better than 0.1% RSD for all Pb ratios.

5. Mineralogy

5.1. Studied samples

During the field and underground studies, the samples were collected from HBF deposits in order to identify the rock units, replacement zones and mineralized veins/veinlets. These samples were systematically obtained from the walls of the actively mined Handeresi, Bağırkaçdere and Fırıncıkdere adits to examine the mineralogy, mineral

paragenesis and textural variations across the alteration and mineralization zones. Because the mineralizations are mostly associated with calc-silicate minerals, these zones are termed "ore-alteration zones". Both massive and disseminated Pb–Zn ores in the HBF deposits are hosted by carbonate lenses and veins/veinlets in epidote–sericite–graphite schists of the Kalabak Fm. They also occur at the contact between the schists and the marble lenses. While main gangue minerals are garnet, pyroxene, epidote, actinolite–tremolite, quartz and calcite, main ore minerals are pyrite, sphalerite, galena, chalcopyrite, hematite, arsenopyrite, and magnetite. Prograde stage is characterized by the origin of anhydrous silicate minerals; the retrograde stage brought a succession of increasingly more hydrous phases. The subsequent ore formation was usually obscured by the alterations which occurred at the prograde stage. Figure 6 shows the paragenesis and succession of the minerals associated with ore mineralizations.

5.2. Silicate minerals

Two main types of garnets were distinguished: colourless to brown grossular (Fig. 7a) and a colourless to green andradite. Some grains show oscillatory zoning but more common is a continuous compositional change towards the rims. The outer zone of some andraditic garnets has a grossular composition (Fig. 7b). Garnets occur also as vein fillings in the form of single crystals or aggregates accompanied by quartz and calcite. Epidotization was detected in the outer zone of some garnets. Secondary calcite fillings were observed in the fractures of some garnets.

The johannsenite–hedenbergite pyroxenes are found especially in Handeresi adits (Fig. 7c) as bladed crystals, granular aggregates, and short prisms in a calcite matrix (Fig. 7a). They are medium–coarse grained and pale–dark grey, black, or pink–brown in colour. The radial carbonate crystals are predominantly pseudomorphs of johannsenite–hedenbergite. In addition, chloritization occurred in these minerals. Diopside has been also detected in the alteration zones as colourless subhedral grains. However, it is very rare compared to the johannsenite–hedenbergite.

Clinozoisite and epidote are fine- to medium-grained, anhedral or thin prismatic (Fig. 7d). The two minerals, which usually occur together with calcite and ore-bearing minerals, form inclusions in quartz. Actinolite strongly prevails over tremolite; still both are very rare in the alteration zones. Actinolite–tremolite, which is fine to medium-grained and prismatic–radial shaped, occurs between garnet and ore minerals in conjunction with quartz and/or calcite (Fig. 7e). Locally, effects of chloritization are observed in actinolite–tremolite occurring with ore-bearing minerals.

Quartz-I and calcite-I, associated with ore bearing minerals, are coarse grained, euhedral–subhedral and filling in the space between the ore minerals and/or silicates. Late-stage quartz and calcite (quartz-II and calcite-II) veinlets cut all the earlier minerals and occupy occasionally the schistosity planes (Fig. 7f). No ore-bearing minerals were observed in quartz (quartz-II) and calcite (calcite-II) veinlets.

5.3. Ore mineralogy

Pyrite grains range from several μm to 0.5 mm across; some are skeletal or cataclastic. Pyrite is replaced by other sulphides or these occur in fractures in pyrite. Some fine-grained pyrites are observed among the johannsenites or in the carbonate matrix (Fig. 8a). Based on these features, pyrite is interpreted as the first of sulphide minerals to have crystallized.

Sphalerite is the predominant ore mineral, besides galena, in the HBF deposits. It forms crystals up to several cm in size, poor in iron (0.9–4.7 mol. % FeS) and enclosing chalcopyrite blebs in amount of up to 20–25 vol. % (Fig. 8b). While some sphalerite grains are cut by chalcopyrite veinlets, the others are enclosed in chalcopyrite. In some polished sections, sphalerite is replaced by galena

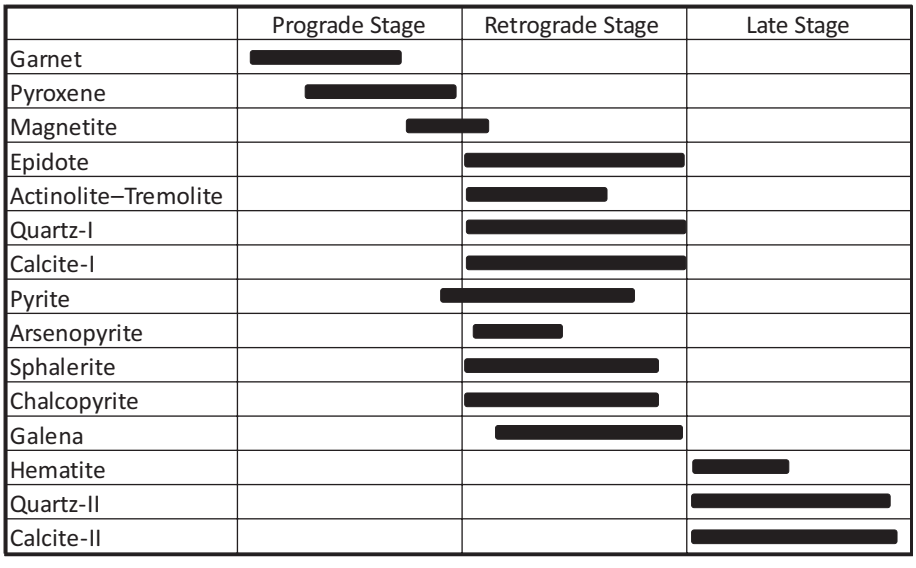

Fig. 6 The paragenesis and the succession of minerals in the HBF deposits.

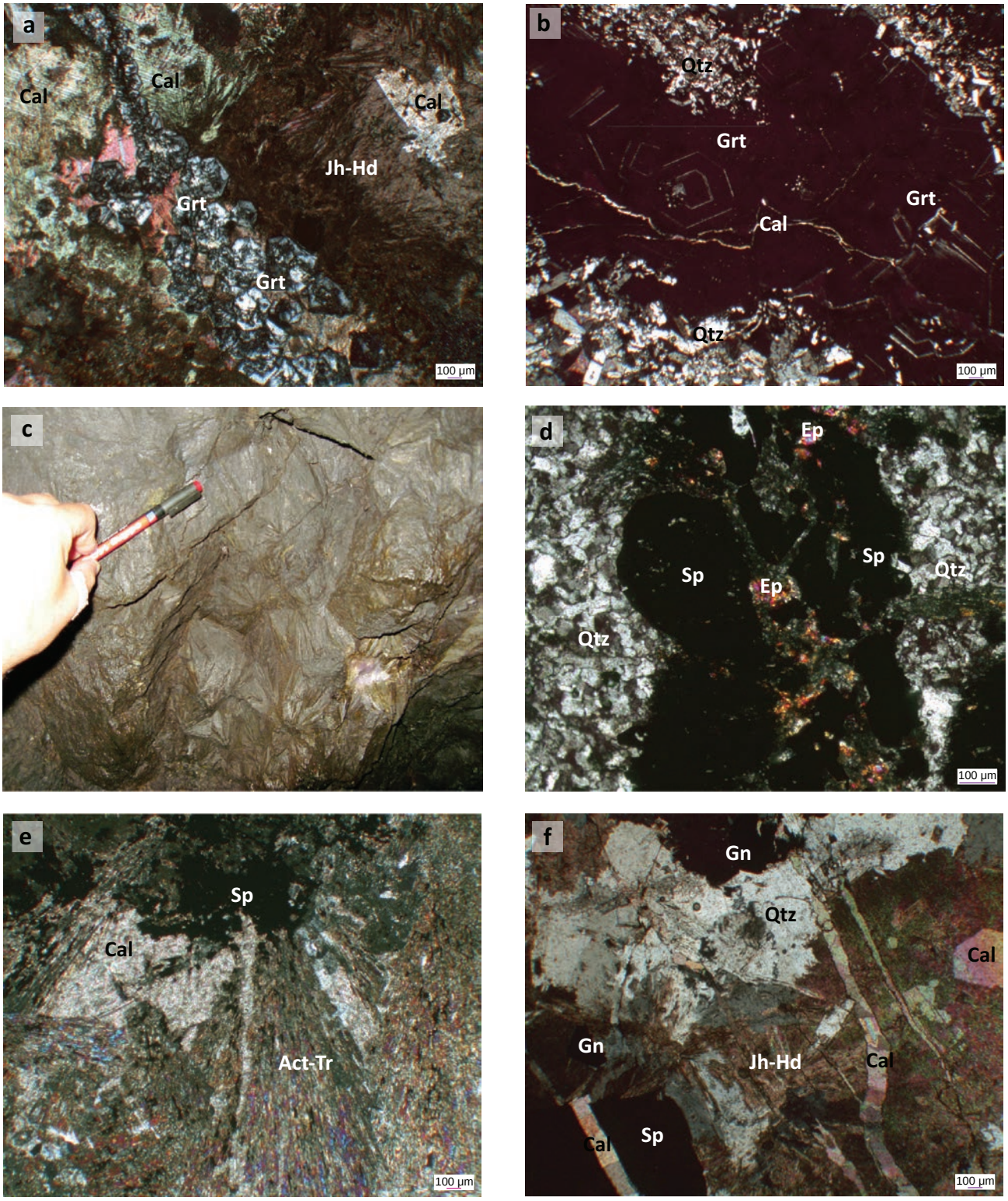

Fig. 7a – Euhedral and subhedral grossular and johannsenite grains (cross-polarized transmitted light, XPL). **b –** Euhedral–subhedral andradite and grossular–andradite (zoned) garnets as vein fillings (XPL). **c –** Coarse-grained johannsenite–hedenbergite forming a zone of 5 meters long in the HDYU adit (in Handeresi area). **d** – Sphalerite crystals as vein-fillings and epidote crystals (XPL). **e** – Radial actinolite–tremolite aggregates with calcite and sphalerite (XPL). **f** – Late-hydrothermal stage quartz-II and calcite-II veinlets (XPL). (abbreviations: Cal: calcite, Grt: garnet, Jh-Hd: johannsenite–hedenbergite, Act–Tr: actinolite–tremolite, Qtz: quartz, Sp: sphalerite, Ep: epidote, Gn: galena).

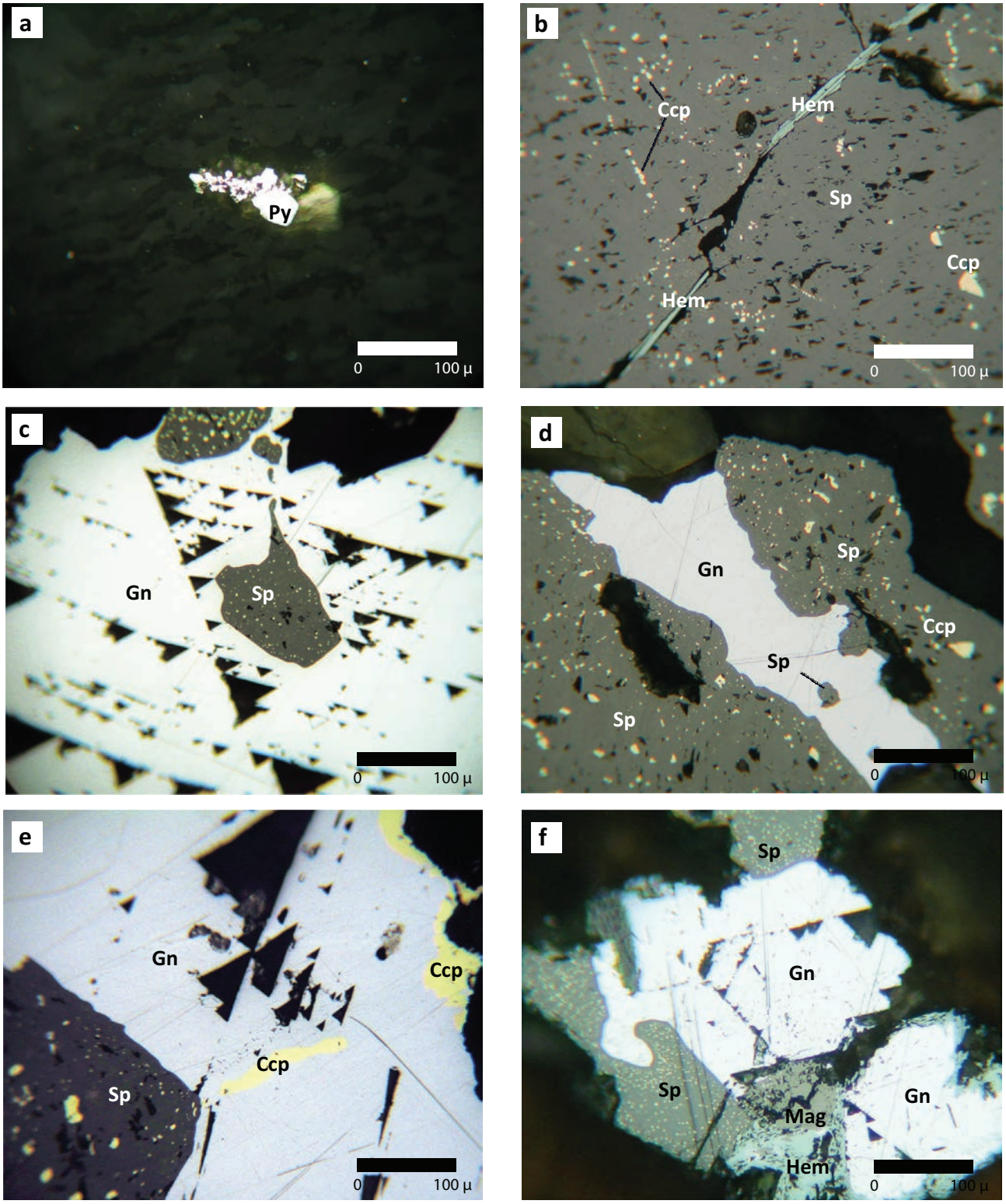

Fig. 8a – Euhedral pyrite crystal in calcite matrix. **b** – Sphalerite grain including the chalcopyrite blebs and radial hematite in cracks. **c** – Galena replacing sphalerite. **d** – Galena forms crack filling in sphalerite and also it contains a sphalerite inclusion. **e** – Chalcopyrite replaces galena. **f** – Hematite surrounding galena crystal and locked magnetite crystal with galena (plain-polarized reflected light), (abbreviations: Py: pyrite, Sp: sphalerite, Ccp: chalcopyrite, Gn: galena, Hem: hematite, Mag: magnetite).

(Fig. 8c). Garnet, epidote, johannsenite–hedenbergite and fibrous hematite occur as inclusions in sphalerite. Quartz-I and calcite-I both infill fractures in sphalerite and the space between sphalerite grains. Arsenopyrite inclusions appear scarcely in some sphalerite grains.

Galena occurs as euhedral–subhedral crystals up to several cm in size. It forms inclusions enclosed in sphalerite, fills in sphalerite fractures or replaces the same phase (Fig. 8d). Chalcopyrite replaces galena and also is observed as crack fillings in the same mineral.

Chalcopyrite forms fine to coarse grains of subhedral–euhedral shapes. It mainly occurs as blebs or grains in sphalerite or as veinlets cutting the same. The distribution of anhedral chalcopyrite blebs resembles "chalcopyrite disease" of Barton and Bethke (1987). Chalcopyrite sometimes occurs as inclusions in galena as well as aggregates surrounding and replacing this mineral (Fig. 8e).

Specularitic hematite forms small grains or radial aggregates (Fig. 8b). While some hematites with quartz occur in cracks in sphalerite and garnet, the others surround the sphalerite, galena and chalcopyrite crystals or attach to them. They also occur in the fractures of epidote, johannsenite–hedenbergite and chlorite.

Arsenopyrite and magnetite are rare. Arsenopyrite occurs as euhedral crystals, some as inclusions in sphalerite. Magnetite forms subhedral–anhedral crystals and grains in galena (Fig. 8f).

6. Mineral chemistry

Table 1 shows the results of the representative EPMA analyses of pyroxene samples. The proportions of johannsenite (Jo), hedenbergite (Hd), and diopside (Di) components in pyroxene are 12.65–35.78, 39.80–52.19 and 23.51–47.54 mol. %, respectively. In the ternary Di–Jo–Hd diagram (Fig. 9a) the samples are restricted to a field of Zn and W skarn deposits reported in the literature (Fig. 9b).

The proportion of the grossular component in garnets ranges between 1 % and 82 % mol. % and the andradite contents between 15 % and 96 % mol. %. Table 2 shows the microprobe analyses of representative garnets. While the Bağırkaçdere and Fırıncıkdere garnets are predominantly of grossular composition, those from Handeresi are richer in the Adr component. Granditic compositions are observed in all the areas. The central part of the BG (Bağırkaçdere) and FD (Fırıncıkdere) garnets are rich in Grs, while their margins are dominated by Adr. The composition of the Handeresi garnet (HD1_c, HD1_o

Tab. 1 Representative electron microprobe analyses of pyroxenes in the HBF deposits (wt. %)

Sample no.	BG1	BG2	BG3	BG4	BG5	FD1	FD2	FD3	HDK1	HDK2
SiO_2	50.25	50.37	50.20	49.41	50.07	49.60	50.67	50.46	49.30	51.70
TiO_2	0.00	0.00	0.00	0.00	0.00	0.00	0.01	0.01	0.00	0.03
Al_2O_3	0.03	0.05	0.07	0.07	0.08	0.07	0.09	0.03	0.10	0.06
FeO(total)	14.47	16.52	15.24	13.52	14.45	14.47	15.18	15.16	15.48	13.04
MnO	8.99	5.91	8.14	10.68	9.11	8.90	4.48	4.78	5.33	4.01
MgO	4.01	4.84	4.37	4.16	3.91	4.03	6.48	6.00	5.32	8.55
CaO	23.03	22.77	23.00	21.96	23.43	23.16	22.85	23.39	22.21	23.01
Na_2O	0.03	0.11	0.09	0.15	0.14	0.08	0.04	0.12	0.08	0.07
K_2O	0.01	0.01	0.01	0.05	0.00	0.01	0.00	0.04	0.00	0.01
Total	100.82	100.58	101.10	100.00	101.20	100.32	99.80	99.99	97.82	100.50
Number of ions on the basis of 6 O										
Si	1.996	1.994	1.984	1.979	1.980	1.978	1.997	1.989	1.997	1.996
Ti	0.000	0.000	0.000	0.000	0.000	0.000	<0.010	<0.010	0.000	0.001
Al	0.001	0.002	0.003	0.003	0.004	0.003	0.004	0.001	0.005	0.003
Fe^{3+}	0.010	0.019	0.036	0.051	0.047	0.046	0.004	0.028	0.008	0.009
Fe^{2+}	0.471	0.528	0.467	0.402	0.431	0.436	0.496	0.471	0.517	0.412
Mn	0.302	0.198	0.272	0.362	0.305	0.301	0.149	0.160	0.183	0.131
Mg	0.238	0.286	0.257	0.249	0.231	0.240	0.381	0.353	0.321	0.492
Ca	0.980	0.966	0.974	0.942	0.992	0.990	0.965	0.988	0.964	0.952
Na	0.002	0.008	0.007	0.012	0.011	0.006	0.003	0.009	0.006	0.005
Sum	4.000	4.000	4.000	4.000	4.000	4.000	4.000	4.000	4.000	4.000
End members (mol. %)										
Wollastonite	58.1	54.3	57.3	59.2	60.0	59.4	52.4	54.5	53.5	51.3
Enstatite	14.1	16.1	15.2	15.6	14.0	14.4	20.7	19.5	17.8	26.5
Ferrosalite	27.9	29.7	27.5	25.2	26.0	26.2	26.9	26.0	28.7	22.2
Mn/Fe	0.642	0.375	0.583	0.902	0.708	0.689	0.301	0.339	0.354	0.318
Mean					0.521					

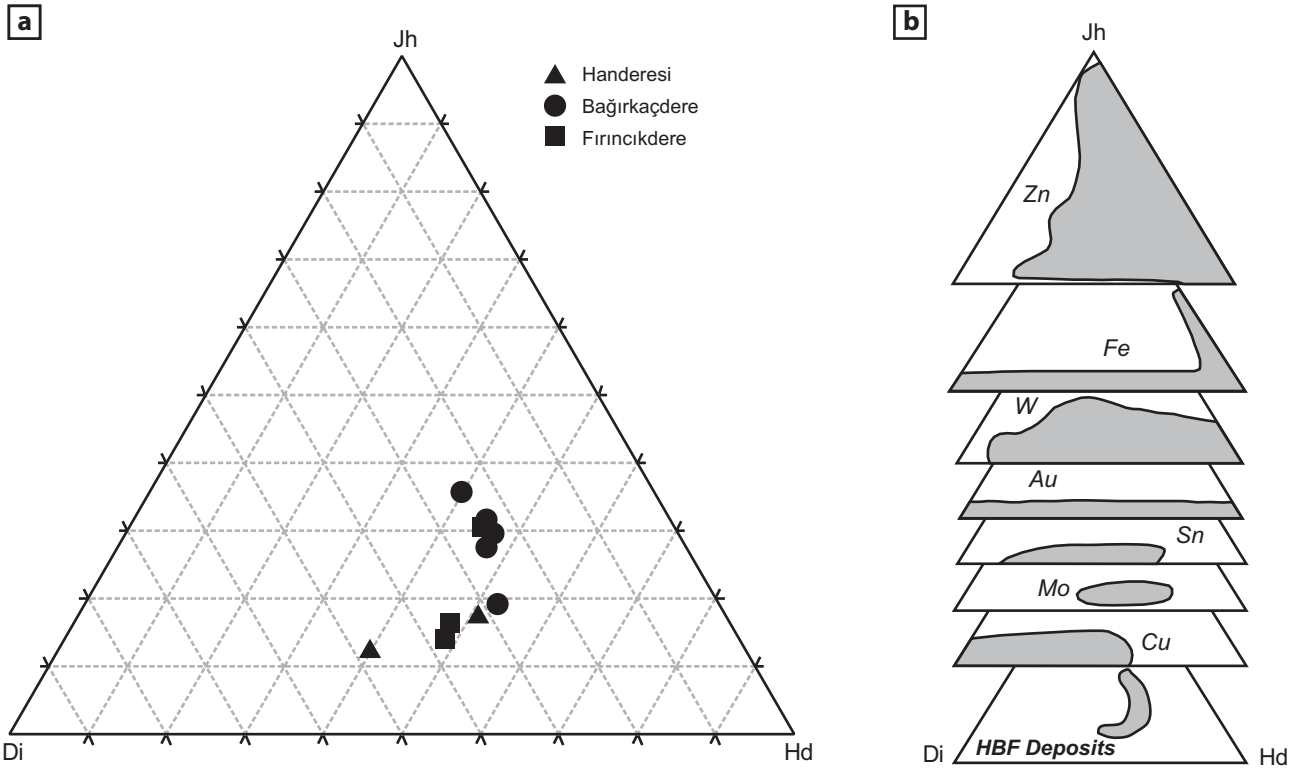

Fig. 9 Ternary diagram of Jh–Di–Hd (johannsenite–diopside–hedenbergite) end-members for the pyroxenes from the HBF deposits (**a**) compared with the world major skarn types (Meinert 1989; Meinert et al. 2005) (**b**).

Tab. 2 Representative microprobe analyses of garnets in the HBF deposits (wt. %)

Sample no.	BG1_c	BG1_e	FD1_c	FD1_e	FD2_c	FD2_e	HD_1_c	HD1_o	HD1_e	HD2_c	HD2_z2	HD2_z1	HD2_e
SiO_2	37.31	36.49	36.68	37.28	36.48	36.45	34.85	34.32	34.38	34.60	34.67	34.75	34.54
TiO_2	0.00	0.04	0.00	0.04	0.09	0.02	0.00	0.00	0.02	0.00	0.00	0.00	0.00
Al_2O_3	17.94	9.31	17.80	13.95	18.95	16.72	4.21	0.54	0.57	0.76	0.41	0.09	2.44
Cr_2O_3	0.00	0.01	0.00	0.00	0.03	0.00	0.01	0.00	0.00	0.00	0.02	0.00	0.02
FeO(total)	6.28	18.26	6.28	11.19	4.91	7.97	22.32	27.83	27.37	27.11	27.82	27.63	25.56
MnO	3.09	0.76	0.93	0.49	1.19	0.83	1.31	0.64	0.73	1.05	0.99	0.56	0.48
MgO	0.03	0.01	0.07	0.05	0.06	0.14	0.00	0.02	0.00	0.02	0.04	0.04	0.00
CaO	34.44	35.84	37.69	35.65	36.94	36.50	33.74	33.34	32.82	33.23	32.96	33.36	33.34
Total	99.09	100.73	99.45	98.63	98.65	98.61	96.44	96.68	95.88	96.77	96.90	96.43	96.37
Number of ions on the basis of 24 O													
Si	5.924	6.087	5.816	6.073	5.782	5.865	6.285	6.377	6.423	6.332	6.422	6.463	6.134
Al	3.358	1.831	3.327	2.678	3.540	3.170	0.894	0.118	0.124	0.526	0.089	0.019	0.158
Ti	0.000	0.005	0.000	0.004	0.011	0.002	0.000	0.000	0.002	0.000	0.000	0.000	0.000
Cr	0.000	0.001	0.000	0.000	0.004	0.000	0.002	0.000	0.000	0.003	0.003	0.000	0.000
Fe	0.833	2.548	0.833	1.524	0.651	1.072	3.367	4.325	4.277	3.919	4.310	4.297	4.020
Mg	0.008	0.002	0.016	0.012	0.014	0.034	0.000	0.006	0.000	0.000	0.012	0.011	0.008
Mn	0.415	0.108	0.125	0.068	0.160	0.113	0.201	0.100	0.115	0.074	0.155	0.088	0.158
Ca	5.860	6.407	6.404	6.223	6.273	6.293	6.519	6.639	6.571	6.548	6.542	6.649	6.312
Sum	16.397	16.991	16.521	16.583	16.435	16.549	17.267	17.564	17.513	17.403	17.532	17.527	16.790
End members (mol. %)													
Almandine	0.0	0.0	0.0	0.0	0.0	0.0	0.0	0.0	0.0	0.0	0.0	0.0	0.0
Pyrope	0.1	0.0	0.3	0.2	0.2	0.5	0.0	0.1	0.0	0.1	0.2	0.2	0.0
Spessartine	6.6	1.7	1.9	1.1	2.5	1.8	3.0	1.5	1.7	2.4	2.3	1.3	1.1
Grossular	73.4	39.6	78.8	62.4	82.0	72.7	21.8	2.2	2.3	4.4	1.1	3.0	10.0
Andradite	19.9	58.6	19.1	36.2	15.1	25.0	75.2	96.2	95.9	93.1	96.4	95.5	88.8
Uvarovite	0.0	0.0	0.0	0.0	0.1	0.0	0.0	0.0	0.0	0.0	0.0	0.0	0.0

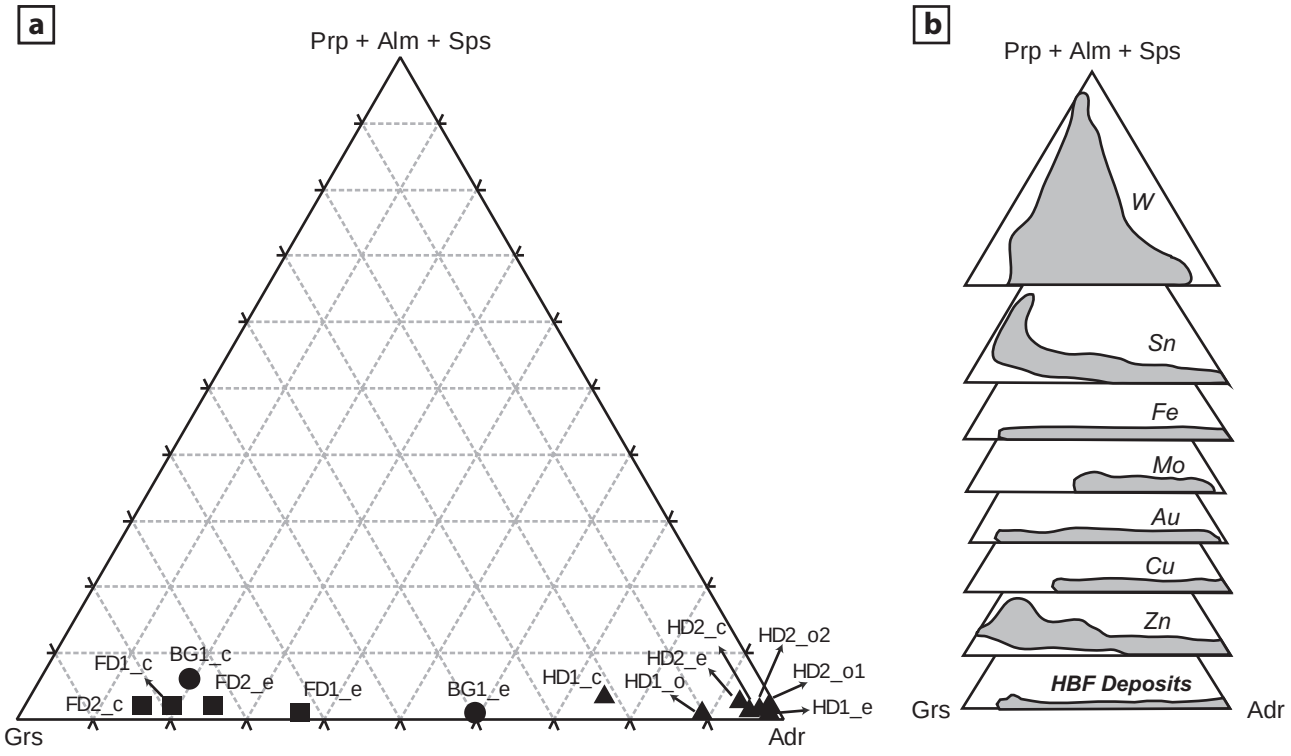

Fig. 10 Ternary diagram of Prp + Alm + Sps–Grs–Adr (pyrope + almandine + spessartine–grossular–andradite) end-members for the garnets from the HBF deposits (**a**) compared to world major skarn types (Meinert 1989; Meinert et al. 2005) (**b**).

and HD1_e; from centre to the margin in the same crystal) is similar to that mentioned previously, but is much more andraditic. The garnet from Handeresi is of almost purely andradite composition (HD2_c, HD2_z2, HD2_z1 and HD2_e; from centre to the margin of one crystal) (Fig. 10a). The Prp + Alm + Sps contents of all garnets are below 10 mol. %. The garnets in HBF Pb–Zn ± Cu deposits fall in Au and Fe skarn fields and show substantial compatibility with the Zn and Cu skarn fields when compared with the major skarn types (Fig. 10b).

7. Isotope data

7.1. Sulphur isotopes

Twenty-six sulphide samples (sphalerite, galena, and chalcopyrite) were analyzed for their sulphur isotope compositions (8: Handeresi, 9: Bağırkaçdere, 9: Fırıncıkdere; Tab. 3).

The sulphur isotope compositions of sulphides range between –1.2 and +2.1 ‰ (mean: +0.6 ‰) in Handeresi, –0.7 and +1.2 ‰ (mean: +0.2 ‰) in Bağırkaçdere and –1.1 and +1.7 ‰ (mean: –0.1 ‰) in Fırıncıkdere areas (Fig. 11a). The $\delta^{34}S$ values for galena fall between –1.1 and +1.5 ‰ (mean: –0.2 ‰), the $\delta^{34}S$ values for sphalerite between –0.7 and + 2.1 ‰ (mean: +0.7 ‰) and for chalcopyrite –0.6 to +1.5 ‰ (mean: +0.4 ‰) (Fig. 11b).

Sulphur isotope temperatures calculated from sphalerite–galena pairs on 4 samples (Akıska 2010; Tab. 3) are fairly high and do not correlate with fluid-inclusion data. Homogenization temperatures of fluid inclusions in sphalerite range from 272 to 338 °C (Akıska et al. 2010; Bozkaya 2011). These significant inconsistencies are interpreted in terms of the coexisting sphalerite–galena pairs isotopic disequilibria (Ohmoto and Rye 1979).

7.2. Lead isotopes

Lead isotope determinations were carried out on five samples (two of galena and three from host rocks). The data are shown in Tab. 4 and plotted in covariation diagrams (Figs 12–13). The lead isotope data for galena show mean values of 18.760, 15.689, and 38.935 for $^{206}Pb/^{204}Pb$, $^{207}Pb/^{204}Pb$, and $^{208}Pb/^{204}Pb$, respectively.

8. Discussion

Distal Pb–Zn skarn deposits are related to the main episodes of continental arc magmatism and intracontinental rifting (Sawkins 1990; Meinert 1992, 1995). The deposits are mostly dominated by Zn accompanied by Pb and Ag.

The grade of these deposits is 10–20 % Zn + Pb and 30–300 g/t Ag. The most important common feature of the distal Pb–Zn skarns in different geological settings is that they occur far from the related igneous rocks (Meinert 1992) and that the relationships between the mineralizations and their presumed parental granitoids cannot be directly observed (Meinert 1992; Baker et al. 2004; Williams-Jones et al. 2010).

In the study area, no spatial relationship between ore-bearing rocks and the nearby Eybek Pluton was observed (Çetinkaya et al. 1983a, b; Tufan 1993; Akıska 2010). Also, any clear link between the mineralizations and the pluton could not be established neither in the adits nor in drill holes (Akıska 2010). However, because the mineralizations are located in close proximity to the Eybek Pluton and the mineral paragenesis related to skarn-type deposits (grossular–andradite, Mn-johannsenite–hedenbergite, epidote–clinozoisite, partly actinolite–tremolite), some indirect relationships can be assumed.

Tab. 3 $\delta^{34}S_{VCDT}$ values of the sulphide samples from the HBF deposits (abbreviations: Ccp: chalcopyrite, Gn: galena, Sp: sphalerite)

Area	Sample No	Elevation	Mineral	$\delta^{34}S_{VCDT}$	Δ_{Sp-Gn}	T (°C)
HANDERESİ	HDHD1	280 m	Ccp	0.2		
	HDK(p)	279 m	Gn	1.5		
	HDK(p)	279 m	Ccp	1.5		
	HDK90	280 m	Sp	2.1	Sp–Gn	542
	HDK90	280 m	Gn	1.0	1.1	
	HDYU91	294 m	Sp	0.4	Sp–Gn	402
	HDYU91	294 m	Gn	–1.2	1.6	
	HDYU95	295 m	Gn	–0.8		
BAĞIRKAÇDERE	AB69	639 m	Sp	1.2		
	BAG07_2	590 m	Gn	–0.7		
	BG64	570 m	Sp	0.1		
	BG66	570 m	Sp	–0.1		
	BG68	570 m	Gn	–0.2		
	BG70	570 m	Ccp	1.0		
	BG71	571 m	Sp	0.8		
	BG72	571 m	Ccp	0.6		
	BG72	571 m	Gn	–0.4		
FIRINCIKDERE	FD07_1	538 m	Gn	–1.1		
	FD07_2	538 m	Sp	1.7	Sp–Gn	364
	FD07_2	538 m	Gn	–0.1	1.8	
	FD07_2	538 m	Ccp	–0.6		
	FD07_3	538 m	Gn	–0.4		
	FD11	541 m	Ccp	–0.4		
	FD11	541 m	Sp	–0.7		
	FD6	540 m	Sp	0.8	Sp–Gn	628
	FD6	540 m	Gn	–0.1	0.9	

Chalcopyrite blebs in sphalerite similar to those observed in our case occur in vein and sea-floor deposits that formed at 200–400 °C (Barton and Bethke 1987).

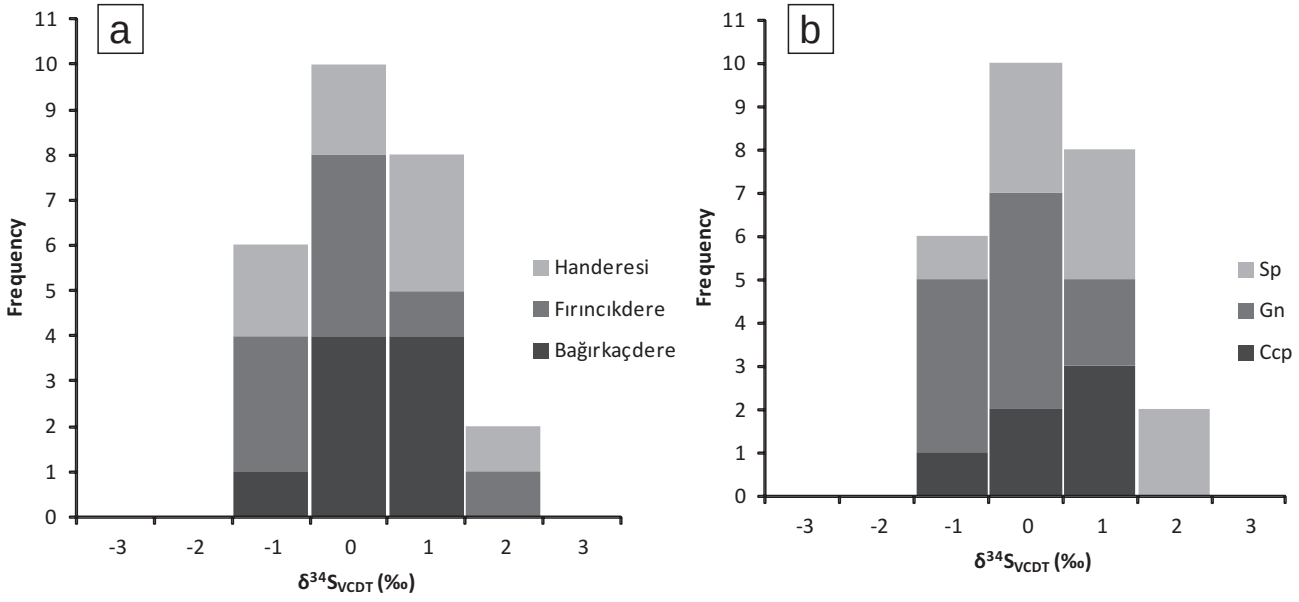

Fig. 11 The frequency histograms showing $\delta^{34}S$ values from individual areas (Handeresi, Bağırkaçdere, and Fırıncıkdere; **a**) and different minerals: sphalerite (Sp), galena (Gn), and chalcopyrite (Ccp) (**b**).

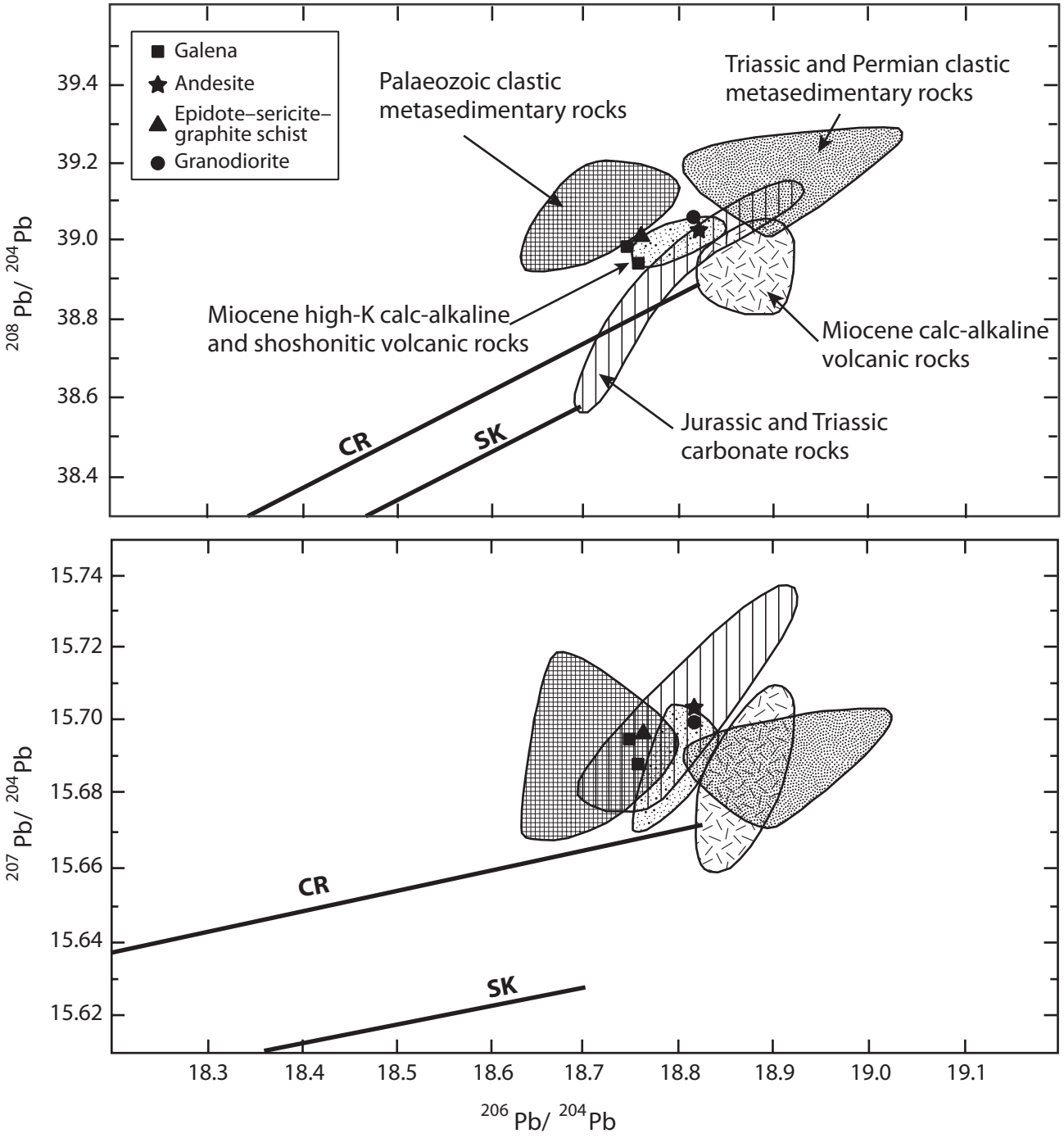

Fig. 12 The thorogenic and uranogenic covariation diagrams. Shaded regions are the lead isotope analyses of various host-rock types from Arribas and Tosdal (1994). (CR: Cumming and Richards (1975), SK: Stacey and Kramers (1975) average crustal Pb growth curves).

Tab. 4 Lead isotope compositions of galenas and the host rocks in the HBF deposits

Sample No	Location	Rock/mineral	$^{206}Pb/^{204}Pb$	$^{207}Pb/^{204}Pb$	$^{208}Pb/^{204}Pb$
1. KAL06	Kalkım volcanics	Andesite	18.83383(±0.0002)	15.70138(±0.00006)	38.98778(±0.0002)
2. HDYU80	Kalabak Fm.	Graphite schist	18.77877(±0.0005)	15.69182(±0.0005)	38.95433(±0.001)
3. EYGR11	Eybek Pluton	Granodiorite	18.83131(±0.001)	15.69472(±0.001)	39.02391(±0.004)
4. HDK(p)	Handeresi Adit	Galena	18.76358(±0.0009)	15.69061(±0.0008)	38.94293(±0.002)
5. FD6	Fırıncıkdere Adit	Galena	18.75607(±0.002)	15.68656(±0.002)	38.92620(±0.005)

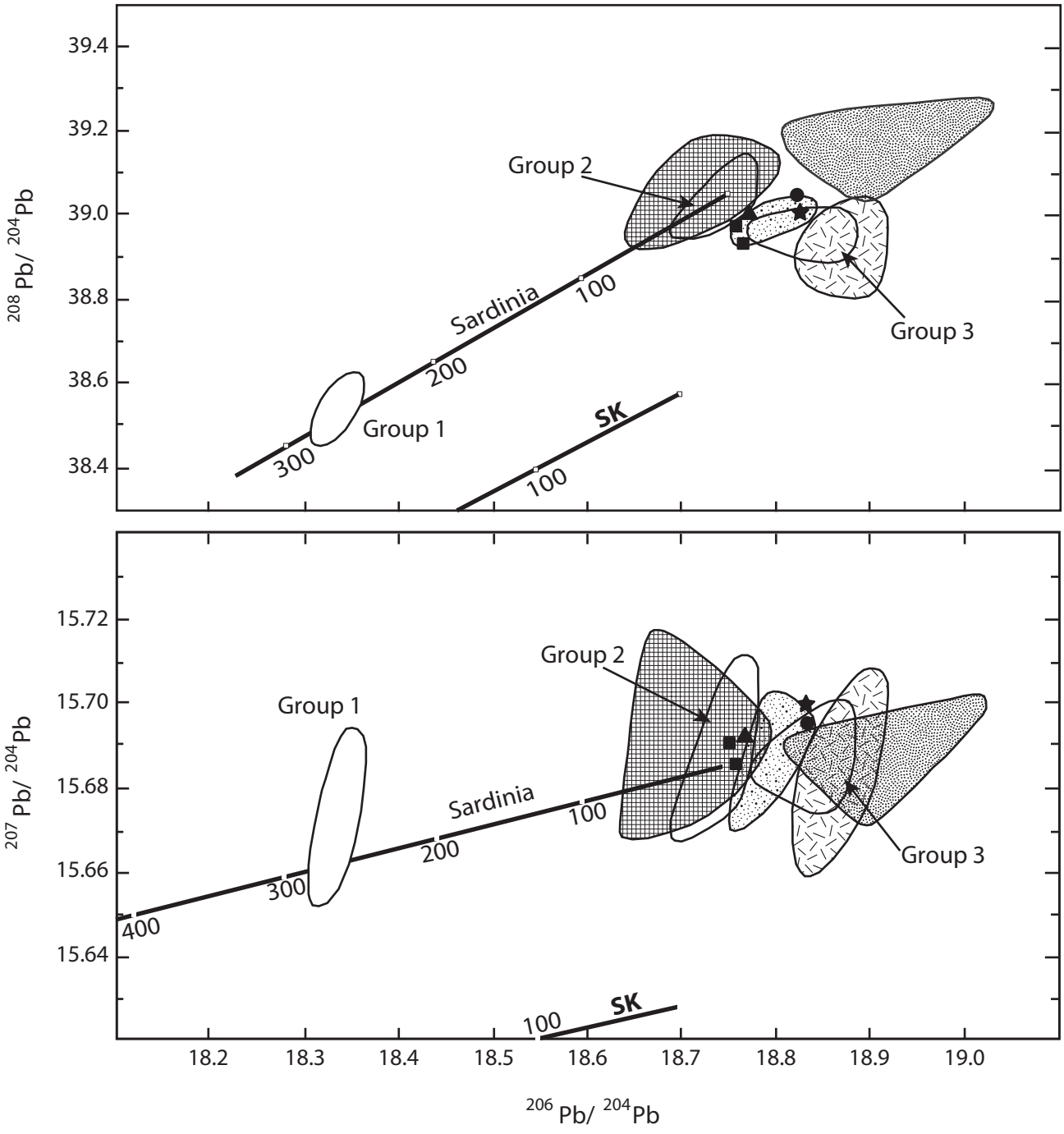

Fig. 13 The thorogenic and uranogenic covariation diagrams. Groups 1–3 are the different types of ore deposits from Arribas and Tosdal (1994). (Sardinia: Ludwig (1989), SK: Stacey and Kramers (1975) average crustal Pb growth curves). (see Fig. 12 for the legend).

These conditions are compatible with the fluid-inclusion homogenization temperatures obtained from the ore-bearing minerals in the study areas (Akıska et al. 2010; Bozkaya 2011). The presence of the grossular–andradite type garnets and hedenbergite–johannsenite type pyroxenes is important because these minerals show that skarns originated in different geochemical environments than other types of Pb–Zn ore formations (e.g. MVT, SEDEX). Besides the Zn–Pb–Ag metal contents, significant Mn- and Fe-rich mineralogy and occurrence along the structural and lithological contacts make distal Pb–Zn skarns distinct from the other type skarn deposits (Meinert 1992). According to some authors, the Mn content in calcic pyroxene, garnet, and chlorite is an important distinguishing feature for Zn skarns (Einaudi et al. 1981; Nakano 1998; Meinert et al. 2005; Canet et al.

2009; Canet et al. 2011). The Mn/Fe ratios of pyroxenes from HBF deposits studied range between 0.3 and 0.9 (mean 0.5) (Tab. 1). Such high Mn/Fe ratios (> 0.2) are typical of Pb–Zn skarn type deposits (Einaudi and Burt 1982; Nakano et al. 1994). The grossular–andradite type garnets that include Mn-rich chemistry also indicate the skarn-type interactions in the study area (Tabs 1–2).

Rye and Ohmoto (1974) showed that some mineralizations including the Providencia (Mexico) and Casapalca (Peru) deposits were related to calc-alkaline intrusives and lack the sulphate minerals. The $\delta^{34}S$ values of these deposits scatter within a narrow range around 0 ‰. Shimazaki and Yamamoto (1979) determined that the sulphur isotope values in some of Japan's skarn-type deposits were very close to 0 ‰ and distributed in a narrow interval of –1.7 to +0.7 ‰. The values in both studies indicated that the magmatic sources are compatible with the $\delta^{34}S$ values which are related with porphyry and skarn type deposits (Ohmoto and Rye 1979). In the current study, the results prove that sulphur came from the same source in all deposits (Handeresi, Bağırkaçdere, and Fırıncıkdere) and the physicochemical environment was not much variable during the ore-forming process.

Because of the similarities in geotectonic environment, wall-rock compositions, source of the metal-bearing fluids and the ore formations, the analyzed samples in this study are correlated with the lead isotope studies of geologically similar areas – e.g. the Betic Cordillera zone in Spain (Arribas and Tosdal 1994). Measured $^{208}Pb/^{204}Pb$ and $^{207}Pb/^{204}Pb$ values plot above the reference crustal Pb growth curve of Stacey and Kramers (1975) (Fig. 12). All the rocks and ores are more radiogenic than the average crustal model growth curves of Stacey and Kramers (1975) and Cumming and Richards (1975). Therefore, the lead of our samples is related to lower crust source (Doe and Zartman 1979). In Figs 12 and 13, one of the studied galena samples nearly coincides with the schist analysis. Also both galena samples fall into, or very close to, the fields of local Palaeozoic clastic metasediments or Miocene K-rich igneous rocks. This means that Pb could have been derived from the schists and/or magmatic rocks.

In Fig. 13, the fields (groups 1–3) show the different types of ore zones in Arribas and Tosdal (1994). The authors stated that the galena samples in Group 2 indicate that the lead in metasedimentary rocks was mobilized by the effect of the volcanism in Miocene epoch adding an amount of magmatic lead. It was also deposited in the rock fractures by the effect of the reactive carbonates.

9. Conclusions

The HBF mineralization in the study area occurs in the carbonate horizons and is controlled both structurally and lithologically. Massive and disseminated Pb–Zn mineralizations are hosted by carbonate lenses, as veins/veinlets in epidote–sericite–graphite schists or they occur at the contact between the schists and the marble lenses and/or calcareous schists. Grossular–andradite, hedenbergite–johannsenite and diopside, epidote–clinozoisite and small amounts of actinolite–tremolite are the gangue minerals while galena, sphalerite, chalcopyrite, pyrite, hematite and arsenopyrite represent the ore minerals.

With regard to (a) the spatial and temporal relationships with wall rocks, (b) structural features, (c) mineralogical and petrographical properties, (d) mineral chemistry and (e) isotopic characteristics, HBF mineralizations show many similarities to distal Pb–Zn skarns. The Pb isotope data and $\delta^{34}S$ values which scatter around 0 ‰ strengthen the argument in which the mineralization may be of magmatic origin. However, part of the lead could have been derived from the graphite schists as well.

Acknowledgements. This study is a part of the Ph.D. thesis of the first author at the Geological Department of Ankara University supervised by third author and also was supported by Scientific Research Office of Ankara University (BAPRO), Project No. 06B4343007. The authors would like to thank Taner Ünlü for critical reading and comments of an early version of the article, İlkay Kuşcu for fruitful discussions in the field, Ahmet Çağatay for helping with the interpretation of polished sections, Jean S. Cline and Haroldo Lledo for sharing significant views and also allowing us to use the EPMA laboratory facilities, and Oreks Co. Ltd. for allowing access to the study area. We are also grateful the reviewers' (Jiří Zachariáš and an anonymous reviewer), handling editor's (Miroslav Štemprok**)** and editor-in-chief's (Vojtěch Janoušek) valuable and helpful comments that improved the manuscript.

References

Akiska S (2010) Cu–Pb–Zn Occurences of the Yenice (Çanakkale) Area. Unpublished Ph.D. thesis, Ankara University, Ankara, pp 1–234 (in Turkish)

Akiska S, Demirela G, Sayili İS, Kuşcu İ (2010) Fluid inclusion and S isotope systematics of some carbonate-related Pb–Zn–Cu mineralizations in NW Anatolia, Turkey. In: Melfos V, Marchev P, Lakova I, Chatzipetros A (eds) Geol Balcanica Abstracts Volume, XIX Congress of the Carpatho-Balkan Geological Association, Thessaloniki, Greece, pp 21

Arribas Jr A, Tosdal RM (1994) Isotopic composition of Pb and S in base- and precious-metal deposits of the Betic Cordillera, Spain: origin and relationship to other European deposits. Econ Geol 89: 1074–1093

Ayan M (1979) Geochronological and petrological studies of the Eybek granodiorite Pluton (Edremit). Commun Fac Sci Univ Ank Sér C 22: 19–31

Aysal N, Ustaömer T, Öngen S, Keskin M, Köksal S, Peytcheva I, Fanning M (2012) Origin of the Early–Middle Devonian magmatism in the Sakarya Zone, NW Turkey: geochronology, geochemistry and isotope systematics. J Asian Earth Sci 45: 201–222

Baker T, Achterberg EV, Ryan CG, Lang JR (2004) Composition and evolution of ore fluids in a magmatic–hydrothermal skarn deposit. Geology 32: 117–120

Barton Jr PB, Bethke PM (1987) Chalcopyrite disease in sphalerite: pathology and epidemiology. Amer Miner 72: 451–467

Bingöl E (1976) Geotectonic evolution of western Anatolia. Bull of MTA 86: 14–34 (in Turkish)

Bozkaya G (2011) Sulfur isotope composition of the Bagirkacdere lead–zinc deposit, Biga Peninsula, Turkey. In: Goldschmidt Conference 2011, Prague, Abstracts. Mineral Mag 75: 571

Canet C, Camprubí A, González-Partida E, Linares C, Alfonso P, Piñeiro-Fernández F, Prol-Ledesma RM (2009) Mineral assemblages of the Francisco I. Madero Zn–Cu–Pb–(Ag) deposit, Zacatecas, Mexico: implications for ore deposit genesis. Ore Geol Rev 35: 423–435

Canet C, González-Partida E, Camprubí A, Castro-Mora J, Romero FM, Prol-Ledesma RM, Linares C, Romero-Guadarrama JA, Sánches-Vargas LI (2011) The Zn–Pb–Ag skarns of Zacatepec, Northeastern Oaxaca, Mexico: a study of mineral assemblages and ore-forming fluids. Ore Geol Rev 39: 277–290

Cavazza W, Okay AI, Zattin M (2009) Rapid Early–Middle Miocene exhumation of the Kazdağ Massif (western Anatolia). Int J Earth Sci 98: 1935–1947

Cumming GL, Richards JR (1975) Ore lead in a continuously changing Earth. Earth Planet Sci Lett 28: 155–171

Çetinkaya N, Karul B, Önal R, Yenigün K (1983a) The geological report of Çanakkale-Yenice-Kalkım-Bağırkaç Dere. Mineral Research and Exploration Institute of Turkey, Report No. 7814, Ankara, pp 1–18 (in Turkish)

Çetinkaya N, Karul B, Önal R, Yenigün K (1983b) Geological report of Çanakkale-Yenice-Kalkım Handeresi Pb–Zn–Cu deposit. Mineral Research and Exploration Institute of Turkey, Report No. 7822, Ankara, pp 1–20 (in Turkish)

Delaloye M, Bingöl E (2000) Granitoids from western and northwestern Anatolia: geochemistry and modeling of geodynamic evolution. Int Geol Rev 42: 241–268

Demirela G (2011) Geology and Genesis of the Çataltepe (Lapseki/Çanakkale) Pb–Zn ± Cu ± Ag Deposit. Unpublished Ph.D. thesis, Ankara University, Ankara, pp 1–220 (in Turkish)

Doe BR, Zartman RE (1979) Plumbotectonics 1: the Phanerozoic. In: Barnes HL (ed) Geochemistry of Hydrothermal Ore Deposits. John Wiley & Sons, New York, pp 22–70

Duru M, Pehlivan S, Dönmez M, Ilgar A, Akçay AE (2007) Geological map of the Balıkesir-İ18 quadrangle. Mineral Research and Exploration Institute of Turkey, Report No. 97, Ankara, pp 1–53 (in Turkish)

Einaudi MT, Burt DM (1982) A special issue devoted to skarn deposits: introduction – terminology, classification and composition of skarn deposits. Econ Geol 77: 745–754

Einaudi MT, Meinert LD, Newberry RJ (1981) Skarn deposits. Econ Geol 75th Anniversary Volume: 317–391

Ercan T (1979) Cenozoic volcanism in western Anatolia, Thrace and the Aegean islands. J Geol Eng 10: 117–137 (in Turkish)

Fytikas M, Giuliani O, Innocenti F, Marinelli G, Mazzuoli R (1976) Geochronological data on recent magmatism of the Aegean Sea. Tectonophysics 31: 29–34

Ketin İ (1966) Tectonic units of Anatolia. Bull of MTA 66: 23–34 (in Turkish)

Krushensky RD, Akçay Y, Karaege E (1971) Geology of an area east of Edremit, Biga Peninsula, NW Turkey. USGS Prof Pap (IR) TU-25 pp 1–132

Krushensky RD (1975) Neogene calc-alkaline extrusive and intrusive rocks of the Karalar-Yeşiller area, Northwest Anatolia, Turkey. Bull Volcanol 39: 336–360

Ludwig KR (1989) Isotopic constraints on the genesis of base-metal ores in southern and central Sardinia. Eur J Mineral 1: 657–666

Meinert LD (1989) Gold skarn deposits – geology and exploration criteria. Econ Geol Monograph 6: 537–552

Meinert LD (1992) Skarns and skarn deposits. Geosci Can 19: 145–162

Meinert LD (1995) Compositional variations of igneous rocks associated with skarn deposits – chemical evidence for a genetic connections between petrogenesis and mineralization. In: Thompson JFH (ed) Magmas, Fluids, and Ore Deposits. Mineralogical Association of Canada, Short Course Series 23: 401–419

Meinert LD, Dipple GM, Nicolescu S (2005) World skarn deposits. Econ Geol 100th Anniversary Volume: pp 299–336 (with Appendices on CD-ROM)

Nakano T, Yoshino T, Shimazaki H, Shimizu M (1994) Pyroxene composition as an indicator in the classification of skarn deposits. Econ Geol 89: 1567–1580

Nakano T (1998) Pyroxene geochemistry as an indicator for skarn metallogenesis in Japan. In: Lentz DR (ed) Mineralized Intrusion-Related Skarn Systems. Mineralogical Association of Canada, Short Course Series 26: 147–167

Ohmoto H, Rye RO (1979) Isotopes of sulfur and carbon. In: Barnes HL (ed) Geochemistry of Hydrothermal Ore Deposits. John Wiley & Sons, New York, pp 509–567

Okay Aİ, Tüysüz O (1999) Tethyan sutures of northern Turkey. In: Durand B, Jolivet L, Horvath F, Seranne

M (eds) The Mediterranean Basins: Tertiary Extension within the Alpine Orogen. Geological Society London, Special Publications 156: 475–515

Okay Aİ, Siyako M, Bürkan KA (1990) Geology and tectonic evolution of the Biga Peninsula. Turk Assoc Petrol Geol Bull 2: 83–121 (in Turkish)

Okay Aİ, Satir M, Maluski H, Siyako M, Monie P, Metzger R, Akyüz S (1996) Paleo- and Neo-Tethyan events in northwest Turkey: geological and geochronological constraints. In: Yin A, Harrison M (eds) Tectonics of Asia. Cambridge University Press, pp 420–441

Okay Aİ, Satir M, Siebel W (2006) Pre-Alpide orogenic events in the Eastern Mediterranean region. In: Gee DG, Stephenson RA (eds) European Lithosphere Dynamics. Geological Society London, Memoirs 32: 389–405

Okay Aİ, Bozkurt E, Satir M, Yiğitbaş E, Crowley QG, Cosmas KS (2008) Defining the southern margin of Avalonia in the Pontides: geochronological data from the Late Proterozoic and Ordovician granitoids from NW Turkey. Tectonophysics 461: 252–264

Rye RO, Ohmoto H (1974) Sulfur and carbon isotopes and ore genesis: a review. Econ Geol 69: 826–842

Sawkins FJ (1990) Metal Deposits in Relation to Plate Tectonics, 2nd edition. Springer-Verlag, New York, pp 1–461

Shimazaki H, Yamamoto M (1979) Sulfur isotope ratios of some Japanese skarn deposits. Geochem J 13: 261–268

Stacey JS, Kramers JD (1975) Approximation of terrestrial lead isotope evolution by two-stage model. Earth Planet Sci Lett 26: 207–221

Şengör AMC, Yilmaz Y (1981) Tethyan evolution of Turkey: a plate tectonic approach. Tectonophysics 75: 181–241

Tufan AE (1993) Geological and petrographical characteristics of the Karaaydın region (Yenice-Çanakkale) with the genetic investigations of lead–zinc occurrences. Unpublished Ph.D. thesis, Selçuk University, Konya, pp 1–158 (in Turkish)

Williams-Jones AE, Samson IM, Ault KM, Gagnon JE, Fryer BJ (2010) The genesis of distal zinc skarns: evidence from the Mochito Deposit, Honduras. Econ Geol 105: 1411–1440

Yücelay MA (1976) The etude of Çanakkale-Kalkım-Handeresi Pb–Zn–Cu deposit. Mineral Research and Exploration Institute of Turkey, Report No. 5720, Ankara, pp 1–26 (in Turkish)

Zimmermann JL, Saupe F, Öngen S, Anil M (1989) Oligocene–Miocene K–Ar ages of the quartz-monzonite stocks from Nevruz–Çakıroba (Yenice, Çanakkale, northwest Turkey). Fifth Meeting of the European Union of Geosciences, Strasbourg, France. Terra Abstracts 1: 354–355